Differentiating Ferroelectric and Nonferroelectric Electromechanical Effects with Scanning Probe Microscopy

Nina Balke,[*,†,‡] Petro Maksymovych,[†,‡] Stephen Jesse,[†,‡] Andreas Herklotz,[§] Alexander Tselev,[†,‡] Chang-Beom Eom,[∥] Ivan I. Kravchenko,[†] Pu Yu,[⊥,#,¶] and Sergei V. Kalinin[†,‡]

[†]The Center for Nanophase Materials Sciences, [‡]Institute for Functional Imaging of Materials, and [§]Materials Science and Technology Division, Oak Ridge National Laboratory, Oak Ridge, Tennessee 37831, United States, [∥]Materials Science and Engineering, University of Wisconsin, Madison, Wisconsin 53706, United States, [⊥]State Key Laboratory of Low-Dimensional Quantum Physics and Department of Physics, Tsinghua University, Beijing 100084, China, [#]Collaborative Innovation Center of Quantum Matter, Beijing 100084, China, and [¶]RIKEN Center for Emergent Matter Science (CEMS), Wako, Saitama 351-0198, Japan

ABSTRACT Ferroelectricity in functional materials remains one of the most fascinating areas of modern science in the past several decades. In the last several years, the rapid development of piezoresponse force microscopy (PFM) and spectroscopy revealed the presence of electromechanical hysteresis loops and bias-induced remnant polar states in a broad variety of materials including many inorganic oxides, polymers, and biosystems. In many cases, this behavior was interpreted as the ample evidence for ferroelectric nature of the system. Here, we systematically analyze PFM responses on ferroelectric and nonferroelectric materials and demonstrate that mechanisms unrelated to ferroelectricity can induce ferroelectric-like characteristics through charge injection and electrostatic forces on the tip. We will focus on similarities and differences in various PFM measurement characteristics to provide an experimental guideline to differentiate between ferroelectric material properties and charge injection. In the end, we apply the developed measurement protocols to an unknown ferroelectric material.

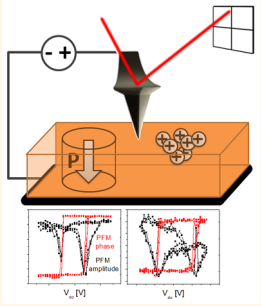

KEYWORDS: scanning probe microscopy · ferroelectricity · electrostatics · relaxors

Ferroelectric materials have remained an area of active research interest since the early 1940s, giving rise to a plethora of applications ranging from sensors and actuators to acoustic imaging and to information technology devices.[1−3] These applications stimulated a broad range of basic science studies of these materials. Actively explored are the limits of ferroelectric phase stability and novel ordering types in low-dimensional systems,[4,5] coupling between ferroelectricity and electronic transport in films and topological defects,[6−11] presence of ferroelectricity in novel material classes including conductive inorganic systems,[12] multiferroic materials,[13] biosystems and polymers,[14] the effect of strain,[15] and structural design of novel ferroelectric heterostructures.[16−18] These necessitate the development of reliable experimental techniques for probing ferroelectricity in functional materials. Relevant approaches include temperature-dependent dielectric permittivity measurements,[19] second harmonic generation,[20,21] as well as classical polarization−electric field ($P-E$) hysteresis measurements with macroscopic electrodes.[1,22] However, these techniques generally require macroscopic materials in the form of electrode devices, whereas probing ferroelectric properties of spatially inhomogeneous and nanoscale systems remains a challenge. The breakthrough in imaging and manipulating of ferroelectric domains and probing polarization dynamics has been achieved with the emergence of piezoresponse force microscopy (PFM), offering the advantages of probing nanometer scale volumes and high-resolution imaging and spectroscopy.

PFM is a scanning probe microscopy (SPM)-based technique which measures the dynamic electromechanical response of the ferroelectric sample when an ac voltage is applied to the SPM tip in mechanical contact with a surface.[23−27] In particular,

* Address correspondence to balken@ornl.gov.

Received for review April 14, 2015 and accepted June 2, 2015.

Published online June 02, 2015
10.1021/acsnano.5b02227

© 2015 American Chemical Society

PFM hysteresis loops in which electromechanical response is measured as a function of applied dc bias, V_{dc}, are often interpreted as an unambiguous indicator of ferroelectricity together with PFM images of ferroelectric domains before or after poling.[14,28−32] However, similar to classical $P−E$ measurements,[22,33] PFM hysteresis loops can originate from a number of alternative mechanisms. For example, electrostatic interactions between tip and sample[34] and hysteretic surface charging[35,36] or ionic mechanism[37−39] can lead to electromechanical hysteresis, as well. The same is true for domain images after poling. Charge writing and strong electrostatic tip−sample interactions can appear as written domains in PFM.[36,40] While, in some cases, the evidence toward the intrinsic ferroelectric nature can be obtained from structural data, for example, direct imaging of switchable polarization by (scanning) transmission electron microscopy,[41−43] this approach is nonuniversal and limited to stable crystalline samples. The existence of nonferroelectric signal contribution in SPM-type experiments is currently under debate;[44] however, clear guidelines on how to avoid or distinguish them from ferroelectric responses is lacking. Here, we report a criterion and measurement schemes for PFM-type experiments to decouple the effect of a switchable polarization and (quasi) permanent surface charges during PFM-type experiments, that is, a behavior unrelated to the presence of ferroelectricity. These studies establish the opportunities and limitations of PFM in probing ferroelectric and other electrochemical responses and will allow for future research in the field of ferroelectrics and other functional materials.

During PFM, a conductive SPM tip is in contact with the sample and an electrical voltage is applied between the SPM tip and the bottom electrode. Due to the inverse piezoelectric effect, the ferroelectric material responds with an expansion or contraction, which is measured as cantilever deflection D through a change in laser spot position on a photodetector. To image domains, an alternating electrical field, V_{ac}, is applied and the ac component of the deflection, D_{ac}, is measured using lock-in techniques. Here, the amplitude and phase of D_{ac} are commonly referred to as the PFM signal, which contains information about the local piezoelectric strength and orientation of the ferroelectric domain. In switching spectroscopy PFM,[45] an additional V_{dc} voltage is applied to the tip in order to change the orientation of the ferroelectric domains. The concurrent detection of PFM signal yields local hysteresis loops. From this, critical switching voltages and measures for switchable polarization can be extracted.[46] In these measurements, V_{ac} and V_{dc} can be applied at the same time (on-field) or subsequently (off-field).[47] In the first case, the domain dynamics are probed under field, whereas in the second, the stability of domains is probed at zero-field after the application of V_{dc} pulses. Note that the identical setup is used in electrochemical strain microscopy (ESM),[37−39] in which case hysteresis loops are associated with a complex set of ionic motion and electrochemical reactions. ESM loops were observed in a variety of materials ranging from room temperature ionic conductors such as Li-ion battery cathodes to cobaltites and manganites used as cathodes in high-temperature solid oxide fuel cells to corresponding electrolytes to electroresistive materials such as $SrTiO_3$, TiO_2, and $LaAlO_3$.[48−51] Remarkably, hysteretic responses are observed for nonferroelectric materials ranging from good ionic conductors to materials where ionic conductivity is expected to be low at room temperature but can be activated by sufficiently high electric fields applied to poor ionic conductors.[52] This comparison undoubtedly reveals that observations of hysteretic responses cannot be used to unambiguously establish their ferroelectric nature and requires alternative methodologies to distinguish ferroelectric from nonferroelectric signal origins in PFM.

As model systems for detailed studies, here we have chosen one ferroelectric and one nonferroelectric thin film. The first sample is epitaxially grown 40 nm tetragonal (001)-oriented $Pb(Zr,Ti)O_3/(La,Sr)MnO_3/SrTiO_3$ (PZT), an example of a classic ferroelectric material. The second one is 10 nm HfO_2 layers grown on Si(100) as the example for a nonferroelectric material. In a previous study, we have shown the dynamic charge storage in this sample using contact Kelvin probe force microscopy (cKPFM).[36] Therefore, this sample is a good model system to show the effect of charge injection and electrostatic forces in PFM measurements. It has been discussed and predicted that HfO_2 can become ferroelectric under certain circumstances,[53−57] which, however, is not the case for the amorphous HfO_2 sample studied here. To this end, different measurements are applied to establish the nature of PFM signals for a 60 nm $SrTiO_3/(Sr,Ca)RuO_3/NdGaO_3$ (STO) sample, which was reported to be a ferroelectric relaxor with a Curie temperature below room temperature. Poled ferroelectric domains and ferroelectric hysteresis loops measured by PFM at room temperature were reported.[58]

RESULTS AND DISCUSSION

First, the similarities in PFM response between HfO_2 and PZT are established. For the HfO_2 and PZT sample, the measured off-field loops show ferroelectric characteristics, such as, butterfly amplitude loops and 180° phase flips when the amplitude is at a minimum (Figure 1a,b). The unfolded off-field and corresponding on-field loops of dynamic deflection as a function of V_{dc} are shown in Figure 1c,d, respectively. In absolute numbers, PZT shows a response higher than that of HfO_2. However, if the measurements are performed with tips of different properties, these differences can vanish or even reverse. The simultaneously measured

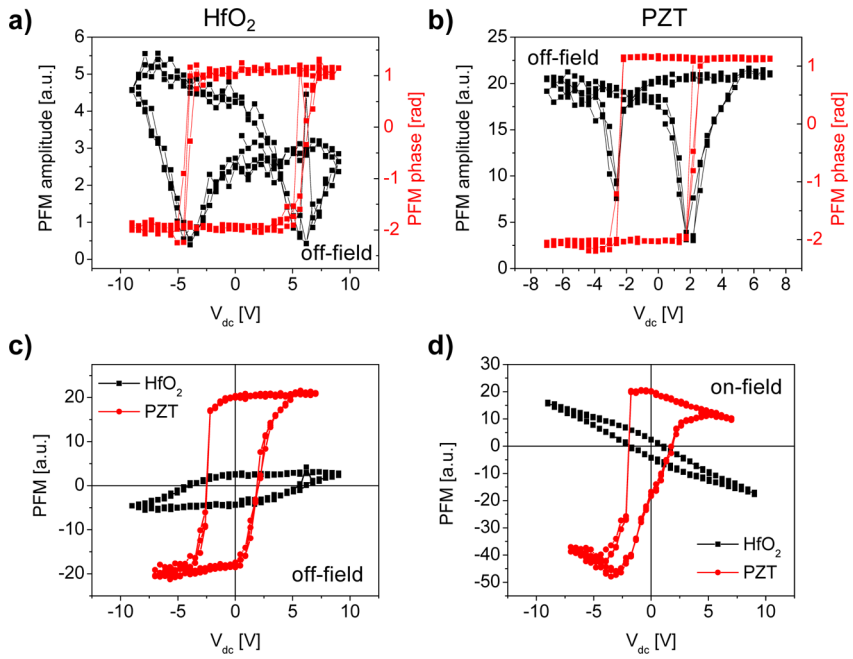

Figure 1. Off-field hysteresis loops separated in amplitude and phase for (a) HfO_2 and (b) PZT. Comparison of (c) off-field loops and (d) on-field loops.

on-field hysteresis loops for these two materials are shown in Figure 1d. For the two materials, the on-field loops are strongly tilted, with visual shape differing due to the difference of the hysteresis component. The slope observed in the on-field loops is ascribed to the presence of electrostatic (ES) forces that can result in a change in measured deflection, which is proportional to the displacement of the cantilever x_{ES}. The slope is mainly affected by the tip−sample contact stiffness and the capacitance gradient of the tip−sample system and varies strongly with tip properties.

Besides the similarities in off-field PFM loops, PFM imaging after poling and PFM relaxation over time are very similar between HfO_2 and PZT. Figure 2 shows the images of PFM amplitude and phase for HfO_2 (Figure 2a−c) and PZT (Figure 2d−f) after poling a small area under a 45° scan angle with positive and negative voltages. The PFM images for HfO_2 were also shown in ref 36. Both PFM amplitude images show zero amplitude regions at the boundary of the switched area with reversed phase contrast, which is typically assigned to be the domain wall. In both cases, the PFM phase reversal after poling is 180°, and only regions with negative poling voltages show a phase inversion. Interestingly, the area poled with positive voltages is visible in the PFM amplitude image for HfO_2 but not for PZT. For the first, the phase inversion comes from the local surface charging, which shifts the electrostatic forces along the voltage axis, as was shown in ref 36. For PZT, the as-grown polarization direction points downward and no polarization reversal happens with positive voltages applied to the scanning tip.

In the case of HfO_2, the injected charges have a relative large lifetime of 1000 s.[36] Therefore, short time relaxation measurements show only small relaxation, which is comparable with PFM relaxation data of PZT (Figure 3). Note that relaxation of the measured signal over long time scales cannot be used to identify charge relaxation in the case of a traditional ferroelectric such as PZT because the instability of switched nanodomains under the biased SPM tip can lead to relaxation, as well. Here, the size of the switched domain determines the relaxation times. Therefore, neither the existence of off-field PFM hysteresis loops, the existence of PFM image contrast after poling, nor the relaxation of the PFM signal is suitable to differentiate between ferroelectric and nonferroelectric sample characteristics.

In the following, the differences in PFM and PFM-like experiments between HfO_2 and PZT are highlighted. As described in ref 36, cKPFM is a PFM-related technique which can be performed in a spectroscopic mode to reveal changes in electrostatic forces after charge injection. The electrostatic signal contribution depends linearly on the applied dc voltage. During a spectroscopic cKPFM experiment, this is denoted as V_{read} to differentiate it from V_{dc}, which is used to induce changes in the surface potential through charge injection. Figure 4a shows the cKPFM curves for HfO_2 after various dc voltage steps between +9 V and −9 V. It can be seen that all curves are linear with a negative slope but show different shifts along the *x*-axis after the dc voltage pulses. This confirms the dominantly electrostatic signal contribution for this sample system and the absence of ferroelectric signal contribution.

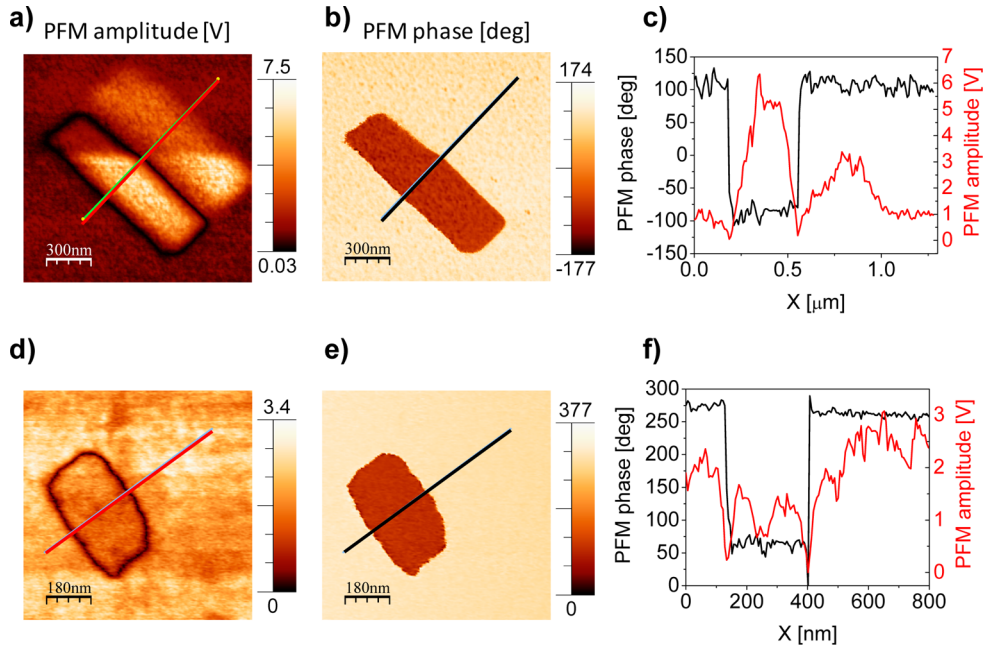

Figure 2. PFM amplitude, PFM phase, and the corresponding line scan through the poled area for HfO_2 (a–c) and PZT (d–f).

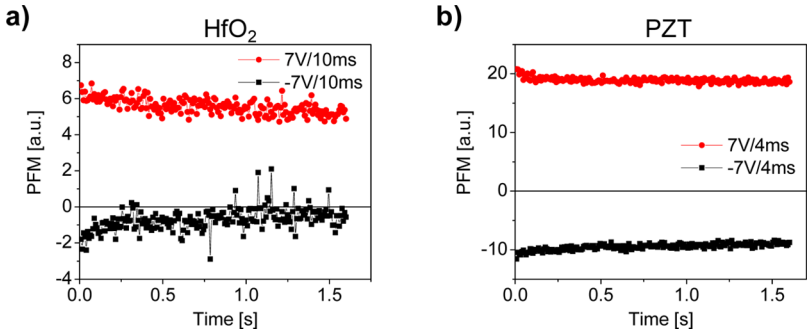

Figure 3. Mixed PFM signal as a function of time after positive and negative voltage pulses for (a) HfO_2 and (b) PZT.

From these, the contact surface potential can be extracted through the intercept of the curve with the *x*-axis. The result is shown in Figure 4b and shows a hysteretic change in surface potential caused by dynamic trapping and detrapping of surface charges.[36] Shown in Figure 2b is also the subsequently measured off-field PFM hysteresis loop. PFM and cKPFM are related techniques, and the PFM signal can be interpreted as the cKPFM measurement at 0 V_{read}. Therefore, a change in surface potential shifts the electrostatic force curve, resulting in a change in *y*-intercept and therefore a measurable change in PFM. Figure 4c displays the macroscopically measured polarization loop after deposition of Pt top electrodes, highlighting the nonferroelectric nature of the amorphous HfO_2 film.

When the experiment is performed on PZT, the cKPFM curves as a function of V_{read} after varying voltage pulses are nonlinear and follow the shape of the hysteresis loop, as shown in Figure 4d. The remnant offset at 0 V is due to the existence of permanent dipoles in the bulk of the material which can be used as an indicator of a ferroelectric material. In addition, it can be observed that the "band" of curves observed for HfO_2 in Figure 4a also exists for PZT. Here, the two bands with two different offsets can be observed, as indicated in Figure 4d. Here we argue that the band formation, as shown in Figure 4a, is universal for all surfaces and is attributable to the injection of charges into the sample surface. The width of the band is the measure of charge injection properties of the surface. In the case of a ferroelectric, the tip field switches ferroelectric domains that extend into the bulk of the sample in addition to the band formation. Hence, the described measurement offers a high-veracity experimental criterion for ferroelectricity in nanoscale systems using SPM.

Other signatures of ferroelectric switching are the loop dependence on the probing ac voltage with respect to the coercive voltages. As demonstrated by Strelcov *et al.*,[59] electromechanical hysteresis loops measured on ferroelectrics change their shape as a

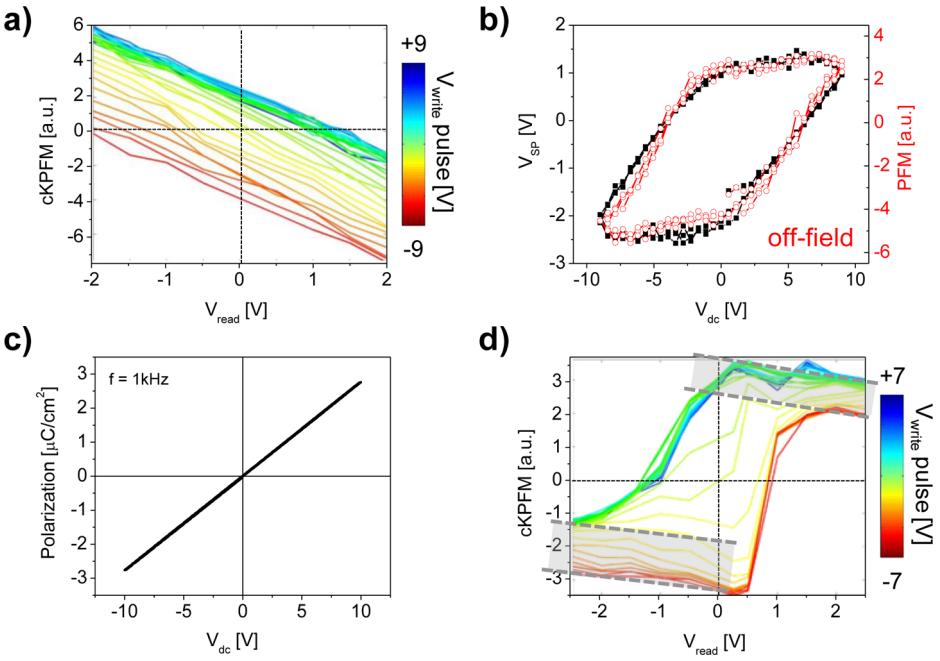

Figure 4. (a) cKPFM curves measured after application of different voltage pulses for HfO_2. (b) Correlation of surface potential, as extracted from panel a, and off-field PFM hysteresis loops. (c) Macroscopically measured polarization loop after deposition of Pt top electrodes measured at 1 kHz. (d) cKPFM curves measured for PZT.

function of V_{ac}. For V_{ac} much smaller than the coercive voltage, the loops are independent of V_{ac}. When the probing voltage approaches the coercive voltage, the effectively measured switching voltages become smaller and eventually (for cases when V_{ac} is larger than the coercive voltage) the ferroelectric loop starts to collapse for the off-field loops and becomes nonhysteretic for the on-field loop.[59] Figure 5 shows the measured on- and off-field loops for HfO_2 and PZT as a function of V_{ac}. While PZT shows the expected behavior for ferroelectrics (Figure 5a,b), the loops measured on HfO_2 seem to be largely independent of V_{ac} (Figure 5c,d). Since the loops are normalized by V_{ac}, this means the measured signal increases linearly with V_{ac} for HfO_2 even for voltages surpassing the measured "switching" voltage.

In the shown examples, ferroelectricity and electrostatics are the main signal contributors. The biggest difference between the origins of these electromechanical signals is that the first originates from an actual volume expansion whereas the second originates from a force acting on the tip. This means that the tip and tip−sample contact properties influence the measurement. As mentioned above, the slope of the electrostatic signal contribution when measured as a function of V_{dc} is proportional to the tip−sample contact stiffness k. The contact stiffness can be increased slightly by using a higher force set-point during the measurement or by using a stiffer cantilever, both evident by a shift of the contact resonance frequency to higher values. For HfO_2, an increase in contact force leads to smaller on- and off-field hysteresis loops with less hysteresis. When using a 10-fold stiffer tip, no measurable signal is detected. On PZT, ferroelectric loops can still be measured with the stiffest tips, and the PFM hysteresis loops increase in area with increasing contact force (not shown here). This ultimately shows that the signal origin in HfO_2 is purely electrostatic in nature and a surface effect. This is supported by the fact that amorphous HfO_2 deposited on a Au bottom electrode yields the same results as shown for HfO_2 without a bottom electrode. However, the exact mechanism of charge injection for different tips and under different contact forces is still poorly understood and will be the subject of future studies.

After important experimental similarities and differences in PFM measurements on ferroelectrics and nonferroelectrics were established, some of the above-described measurements were applied to STO/NGO, whose ferroelectric properties at room temperature are under discussion. This sample was intensively studied in ref 58 by optical and electrical measurements, and it was concluded that the sample shows a relaxor-type ferroelectric behavior. As evident in Figure 6a, the off-field PFM hysteresis loops are the same as those measured on HfO_2 or PZT (compare to Figure 1). The cKPFM curves (Figure 6b) reveal characteristics similar to those of PZT but without a strong remanence of the induced polarization. The reason for this is revealed by the PFM signal relaxation after positive and negative voltage pulses (Figure 6c) which relax very quickly within 1 s. The data for STO/NGO could be explained by a bias-induced dipole orientation

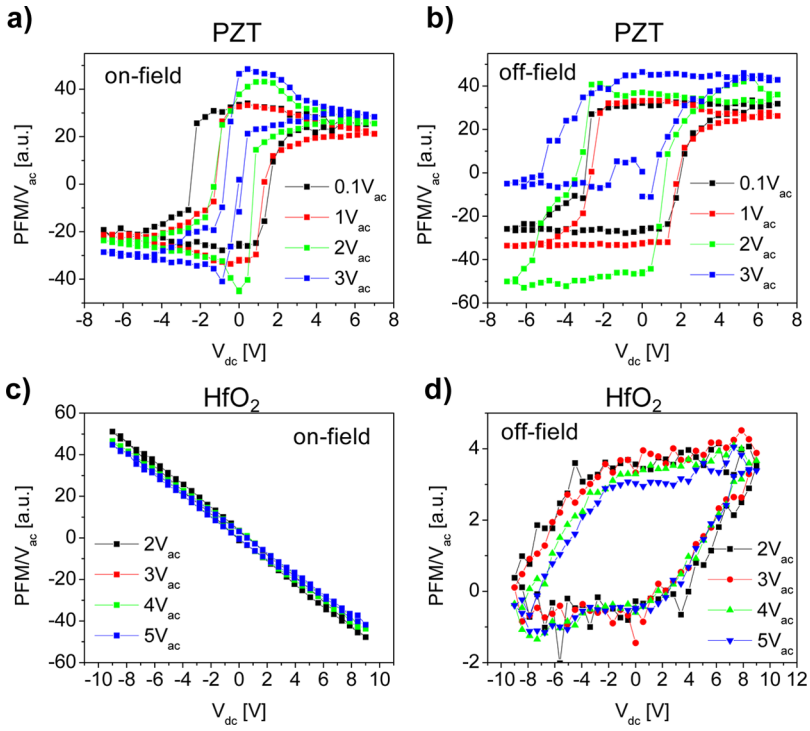

Figure 5. (a) On-field and (b) off-field PFM hysteresis loops as a function of V_{ac} for PZT. (c) On-field and (d) off-field PFM hysteresis loops as a function of V_{ac} for HfO_2. All measured PFM values are normalized by V_{ac}.

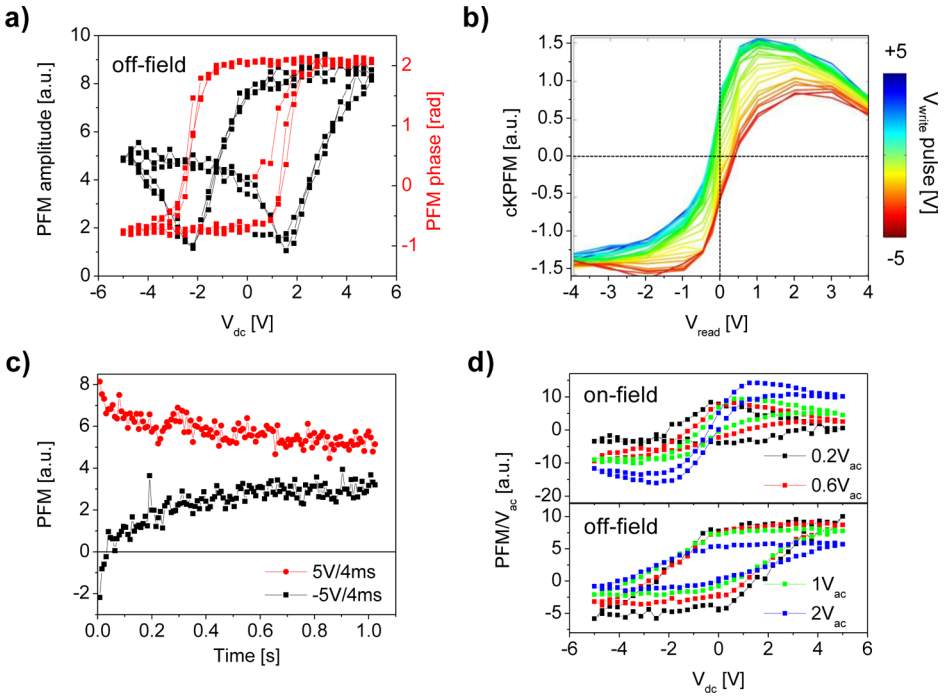

Figure 6. (a) Off-field PFM amplitude and PFM phase hysteresis loops, (b) cKPFM curves, (c) PFM relaxation after dc voltage pulses, and (d) on-field and off-field PFM hysteresis loops as a function of V_{ac} for STO/NGO.

which is not stable at 0 V, as expected for a ferroelectric relaxor. In ferroelectrics, spontaneous polarization, P_s, is defined on the unit cell level, generally has strong crystallographic anisotropy, and adopts well-defined values. In ferroelectric relaxors and electrochemical systems,[60] P_s has no specific orientation and can adopt a continuous spectrum of values. When investigating the V_{ac} dependence of PFM hysteresis loops (Figure 6d), the on-field hysteresis loops change as expected for a ferroelectric material, but the transition between off-field hysteresis loops measured with different V_{ac} is more continuous than for the ferroelectric

material. This finding supports the idea of a relaxor-like behavior at room temperature where the ferroelectric polarizations do not have a fixed direction or strength and is consistent with previous experiments.[58] This example highlights the versatility of the presented experimental approach for a variety of material classes.

CONCLUSIONS

To summarize, we demonstrate how to differentiate between ferroelectric and nonferroelectric electromechanical signal origins in SPM-based characterization techniques. We demonstrated several methods to differentiate the universal signatures of long-range dipoles (ferroelectric polarization) and charge injection at the surface of the sample: (a) cKPFM experiments with varying V_{read}, (b) use of a range of the probing V_{ac} voltage amplitudes, (c) performing measurements with different tip−sample contact stiffnesses. We applied these PFM-based methods to a nonferroelectric material (amorphous, undoped HfO_2) and a classical ferroelectric material (PZT). Both systems show electromechanical hysteresis loops with ferroelectric characteristics when traditional electromechanical hysteresis loops are measured despite the different sample properties. The same applies for PFM images after poling experiments or relaxation of PFM signals after short poling pulses. However, cKPFM experiments or loop shape dependence on probing ac voltage amplitude reveal very different signatures for both samples depending on the origin of the observed signals. The same experiments applied to STO/NGO showed characteristics of a ferroelectric relaxor even at room temperature. The set of experiments we propose to identify ferroelectric signal origins is critical when studying newly developed ferroelectric materials since simple PFM hysteresis loops can have multiple signal origins and cannot be used exclusively to establish ferroelectric material properties. The approaches applied here are focused on the differentiation between ferroelectric and nonferroelectric signal origins. In the future, this will not only help to study new ferroelectric materials or ferroelectricity induced by external parameters but also open PFM-type experiments to other applications of functional oxides.

EXPERIMENTAL SECTION

Switching spectroscopy piezoresponse force microscopy is implemented on a commercial SPM system (Bruker Dimension Icon) inside a glovebox equipped with external data acquisition electronics based on a NI-6115 DAQ card to generate the probing signal and store local hysteresis loops. The hysteresis loop measurements were performed on a 5 × 5 grid with a 1 μm × 1 μm area and averaged. For all measurements, band excitation techniques[61] are used, and the measured contact resonance peaks are fitted to a simple harmonic oscillator to extract the surface oscillation D_{ac}. PFM imaging was performed with a single frequency close to the contact resonance frequency with 1 V_{ac}.

Macroscopic polarization measurements were performed after deposition of 300 × 200 μm Pt top electrodes with an aixACT TF Analyzer 2000 at a frequency of 1 kHz.

The PZT sample with a thickness of 30 nm was grown by pulsed laser deposition on the $SrTiO_3$(001) substrate, with a 20 nm $La_{0.7}Sr_{0.3}MnO_3$ (LSMO) buffered layer as the bottom electrode. The growth conditions were 700 °C and 300 mTorr oxygen pressure for LSMO and 630 °C and 100 mTorr for PZT. After the growth, the film was cooled from growth temperature to room temperature with the ramping rate of 5 °C/min with an oxygen ambient pressure of 1 atm.

The syntheses of the HfO_2 and STO samples are described in refs 36 and 58, respectively.

Conflict of Interest: The authors declare no competing financial interest.

Acknowledgment. Support was provided by the U.S. Department of Energy, Basic Energy Sciences, through the Office of Science Early Career Research Program (N.B.) and the Materials Sciences and Engineering Division (S.V.K., P.M.). The experiments were performed at the Center for Nanophase Materials Sciences, which is a DOE Office of Science User Facility which also provided additional support (S.J., A.T., I.I.K.). P.Y. was financially supported by the National Basic Research Program of China (Grant 2015CB921700) and National Natural Science Foundation of China (Grant 11274194). The work at University of Wisconsin—Madison was supported by the National Science Foundation DMREF (Grant No. DMR-1234096). The authors gratefully acknowledge multiple discussions with A. Gruverman (UNL), R. Proksch (Asylum Research), J. Li (UWash), D. Damjanovic (EPFL), and A. Morozovska (UAS). N.B., P.M., and S.J. designed the experimental concept. N.B. conducted the measurements. S.J. designed the measurement program. A.H. conducted the polarization measurement. C.B.E., P.Y., and I.I.K. provided the samples. All authors discussed and interpreted the experimental results.

REFERENCES AND NOTES

1. Lines, M. E.; Glass, A. M. *Principles and Applications of Ferroelectrics and Related Materials*; Oxford University Press: Oxford, U.K., 1977.
2. Scott, J. F.; De Araujo, C. A. P. Ferroelectric Memories. *Science* **1989**, *246*, 1400–1405.
3. Jona, F.; Shirane, G. *Ferroelectric Crystals*; Dover: New York, 1993; Vol. 108.
4. Naumov, I. I.; Bellaiche, L.; Fu, H. X. Unusual Phase Transitions in Ferroelectric Nanodisks and Nanorods. *Nature* **2004**, *432*, 737–740.
5. Fong, D. D.; Stephenson, G. B.; Streiffer, S. K.; Eastman, J. A.; Auciello, O.; Fuoss, P. H.; Thompson, C. Ferroelectricity in Ultrathin Perovskite Films. *Science* **2004**, *304*, 1650–1653.
6. Seidel, J.; Martin, L. W.; He, Q.; Zhan, Q.; Chu, Y. H.; Rother, A.; Hawkridge, M. E.; Maksymovych, P.; Yu, P.; Gajek, M.; et al. Conduction at Domain Walls in Oxide Multiferroics. *Nat. Mater.* **2009**, *8*, 229–234.
7. Maksymovych, P.; Jesse, S.; Yu, P.; Ramesh, R.; Baddorf, A. P.; Kalinin, S. V. Polarization Control of Electron Tunneling into Ferroelectric Surfaces. *Science* **2009**, *324*, 1421–1425.
8. Sluka, T.; Tagantsev, A. K.; Damjanovic, D.; Gureev, M.; Setter, N. Enhanced Electromechanical Response of Ferroelectrics Due to Charged Domain Walls. *Nat. Commun.* **2012**, *3*, 748.
9. Tsymbal, E. Y.; Kohlstedt, H. Applied Physics: Tunneling across a Ferroelectric. *Science* **2006**, *313*, 181–183.
10. Guyonnet, J.; Gaponenko, I.; Gariglio, S.; Paruch, P. Conduction at Domain Walls in Insulating $Pb(Zr_{0.2}Ti_{0.8})O_3$ Thin Films. *Adv. Mater.* **2011**, *23*, 5377.

11. Gajek, M.; Bibes, M.; Fusil, S.; Bouzehouane, K.; Fontcuberta, J.; Barthelemy, A. E.; Fert, A. Tunnel Junctions with Multiferroic Barriers. *Nat. Mater.* **2007**, *6*, 296–302.
12. Figueiras, F. G. N.; Bdikin, I. K.; Amaral, V. B. S.; Kholkin, A. L. Local Bias Induced Ferroelectricity in Manganites with Competing Charge and Orbital Order States. *Phys. Chem. Chem. Phys.* **2014**, *16*, 4977–4981.
13. Spaldin, N. A.; Fiebig, M. The Renaissance of Magnetoelectric Multiferroics. *Science* **2005**, *309*, 391–392.
14. Liu, Y.; Zhang, Y.; Chow, M.-J.; Chen, Q. N.; Li, J. Biological Ferroelectricity Uncovered in Aortic Walls by Piezoresponse Force Microscopy. *Phys. Rev. Lett.* **2012**, *108*, 078103.
15. Martin, L. W.; Chu, Y. H.; Ramesh, R. Advances in the Growth and Characterization of Magnetic, Ferroelectric, and Multiferroic Oxide Thin Films. *Mater. Sci. Eng., R* **2010**, *68*, 111–133.
16. Martin, L. W.; Schlom, D. G. Advanced Synthesis Techniques and Routes to New Single-Phase Multiferroics. *Curr. Opin. Solid State Mater. Sci.* **2012**, *16*, 199–215.
17. Ramesh, R.; Aggarwal, S.; Auciello, O. Science and Technology of Ferroelectric Films and Heterostructures for Nonvolatile Ferroelectric Memories. *Curr. Opin. Solid State Mater. Sci.* **2001**, *32*, 191–236.
18. Lee, H. N.; Christen, H. M.; Chisholm, M. F.; Rouleau, C. M.; Lowndes, D. H. Strong Polarization Enhancement in Asymmetric Three-Component Ferroelectric Superlattices. *Nature* **2005**, *433*, 395–399.
19. Haeni, J. H.; Irvin, P.; Chang, W.; Uecker, R.; Reiche, P.; Li, Y. L.; Choudhury, S.; Tian, W.; Hawley, M. E.; Craigo, B.; et al. Room-Temperature Ferroelectricity in Strained $SrTiO_3$. *Nature* **2004**, *430*, 758–761.
20. Gopalan, V.; Raj, R. Domain Structure and Phase Transitions in Epitaxial $KNbO_3$ Thin Films Studied by in Situ Second Harmonic Generation Measurements. *Appl. Phys. Lett.* **1996**, *68*, 1323–1325.
21. Lee, C. H.; Skoromets, V.; Biegalski, M. D.; Lei, S. M.; Haislmaier, R.; Bernhagen, M.; Uecker, R.; Xi, X. X.; Gopalan, V.; Marti, X.; et al. Effect of Stoichiometry on the Dielectric Properties and Soft Mode Behavior of Strained Epitaxial $SrTiO_3$ Thin Films on $DyScO_3$ Substrates. *Appl. Phys. Lett.* **2013**, *102*, 082905.
22. Scott, J. F. Ferroelectrics Go Bananas. *J. Phys.: Condens. Matter* **2008**, *20*, 021001.
23. Kholkin, A. L.; Shvartsman, V. V.; Kiselev, D. A. Nanoscale Characterization of Ferroelectric Materials for Piezoelectric Applications. *Ferroelectrics* **2006**, *341*, 3–19.
24. Gruverman, A.; Auciello, O.; Tokumoto, H. Imaging and Control of Domain Structures in Ferroelectric Thin Films via Scanning Force Microscopy. *Annu. Rev. Mater. Sci.* **1998**, *28*, 101–123.
25. Kalinin, S. V.; Rodriguez, B. J.; Jesse, S.; Shin, J.; Baddorf, A. P.; Gupta, P.; Jain, H.; Williams, D. B.; Gruverman, A. Vector Piezoresponse Force Microscopy. *Microsc. Microanal.* **2006**, *12*, 206–220.
26. Kolosov, O.; Gruverman, A.; Hatano, J.; Takahashi, K.; Tokumoto, H. Nanoscale Visualization and Control of Ferroelectric Domains by Atomic-Force Microscopy. *Phys. Rev. Lett.* **1995**, *74*, 4309–4312.
27. Balke, N.; Bdikin, I.; Kalinin, S. V.; Kholkin, A. L. Electromechanical Imaging and Spectroscopy of Ferroelectric and Piezoelectric Materials: State of the Art and Prospects for the Future. *J. Am. Ceram. Soc.* **2009**, *92*, 1629–1647.
28. Bdikin, I. K.; Gracio, J.; Ayouchi, R.; Schwarz, R.; Kholkin, A. L. Local Piezoelectric Properties of ZnO Thin Films Prepared by RF-Plasma-Assisted Pulsed-Laser Deposition Method. *Nanotechnology* **2010**, *21*, 235703.
29. Deepak, N.; Caro, M. A.; Keeney, L.; Pemble, M. E.; Whatmore, R. W. Interesting Evidence for Template-Induced Ferroelectric Behavior in Ultra-thin Titanium Dioxide Films Grown on (110) Neodymium Gallium Oxide Substrates. *Adv. Funct. Mater.* **2014**, *24*, 2844–2851.
30. Herng, T. S.; Kumar, A.; Ong, C. S.; Feng, Y. P.; Lu, Y. H.; Zeng, K. Y.; Ding, J. Investigation of the Non-volatile Resistance Change in Noncentrosymmetric Compounds. *Sci. Rep.* **2012**, *2*, 587.
31. Kolobov, A. V.; Kim, D. J.; Giussani, A.; Fons, P.; Tominaga, J.; Calarco, R.; Gruverman, A. Ferroelectric Switching in Epitaxial Gete Films. *APL Mater.* **2014**, *2*, 066101.
32. Varghese, J.; Barth, S.; Keeney, L.; Whatmore, R. W.; Holmes, J. D. Nanoscale Ferroelectric and Piezoelectric Properties of Sb_2S_3 Nanowire Arrays. *Nano Lett.* **2012**, *12*, 868–872.
33. Jin, L.; Li, F.; Zhang, S. Decoding the Fingerprint of Ferroelectric Loops: Comprehension of the Material Properties and Structures. *J. Am. Ceram. Soc.* **2014**, *97*, 1–27.
34. Kalinin, S. V.; Bonnell, D. A. Contrast Mechanism Maps for Piezoresponse Force Microscopy. *J. Mater. Res.* **2002**, *17*, 936–939.
35. Li, Q.; Liu, Y.; Wang, D. Y.; Withers, R. L.; Li, Z. R.; Luo, H. S.; Xu, Z. Switching Spectroscopic Measurement of Surface Potentials on Ferroelectric Surfaces via an Open-Loop Kelvin Probe Force Microscopy Method. *Appl. Phys. Lett.* **2012**, *101*, 242906.
36. Balke, N.; Maksymovych, P.; Jesse, S.; Kravchenko, I.; Li, Q.; Kalinin, S. V. Exploring Local Electrostatic Effects with Scanning Probe Microscopy: Implications for Piezoresponse Force Microscopy and Triboelectricity. *ACS Nano* **2014**, *8*, 10229–10236.
37. Balke, N.; Jesse, S.; Morozovska, A. N.; Eliseev, E.; Chung, D. W.; Kim, Y.; Adamczyk, L.; Garcia, R. E.; Dudney, N.; Kalinin, S. V. Nanoscale Mapping of Ion Diffusion in a Lithium-Ion Battery Cathode. *Nat. Nanotechnol.* **2010**, *5*, 749–754.
38. Balke, N.; Jesse, S.; Kim, Y.; Adamczyk, L.; Tselev, A.; Ivanov, I. N.; Dudney, N. J.; Kalinin, S. V. Real Space Mapping of Li-Ion Transport in Amorphous Si Anodes with Nanometer Resolution. *Nano Lett.* **2010**, *10*, 3420–3425.
39. Balke, N.; Kalnaus, S.; Dudney, N. J.; Daniel, C.; Jesse, S.; Kalinin, S. V. Local Detection of Activation Energy for Ionic Transport in Lithium Cobalt Oxide. *Nano Lett.* **2012**, *12*, 3399–3403.
40. Khim, Z. G.; Hong, J. Dynamic-Contact Electrostatic Force Microscopy and Its Application to Ferroelectric Domain. *Nanoscale Phenomena in Ferroelectric Thin Films*; Springer: Berlin, 2004; pp 157−182.
41. Jia, C. L.; Mi, S. B.; Urban, K.; Vrejoiu, I.; Alexe, M.; Hesse, D. Atomic-Scale Study of Electric Dipoles near Charged and Uncharged Domain Walls in Ferroelectric Films. *Nat. Mater.* **2008**, *7*, 57–61.
42. Chisholm, M. F.; Luo, W. D.; Oxley, M. P.; Pantelides, S. T.; Lee, H. N. Atomic-Scale Compensation Phenomena at Polar Interfaces. *Phys. Rev. Lett.* **2010**, *105*, 197602.
43. Chang, H. J.; Kalinin, S. V.; Yang, S.; Yu, P.; Bhattacharya, S.; Wu, P. P.; Balke, N.; Jesse, S.; Chen, L. Q.; Ramesh, R.; et al. Watching Domains Grow: In-Situ Studies of Polarization Switching by Combined Scanning Probe and Scanning Transmission Electron Microscopy. *J. Appl. Phys.* **2011**, *110*, 052014.
44. Bark, C. W.; Sharma, P.; Wang, Y.; Baek, S. H.; Lee, S.; Ryu, S.; Folkman, C. M.; Paudel, T. R.; Kumar, A.; Kalinin, S. V.; et al. Switchable Induced Polarization in $LaAlO_3/SrTiO_3$ Heterostructures. *Nano Lett.* **2012**, *12*, 1765–1771.
45. Jesse, S.; Rodriguez, B. J.; Choudhury, S.; Baddorf, A. P.; Vrejoiu, I.; Hesse, D.; Alexe, M.; Eliseev, E. A.; Morozovska, A. N.; Zhang, J.; et al. Direct Imaging of the Spatial and Energy Distribution of Nucleation Centres in Ferroelectric Materials. *Nat. Mater.* **2008**, *7*, 209–215.
46. Jesse, S.; Lee, H. N.; Kalinin, S. V. Quantitative Mapping of Switching Behavior in Piezoresponse Force Microscopy. *Rev. Sci. Instrum.* **2006**, *77*, 073702.
47. Hong, S.; Woo, J.; Shin, H.; Jeon, J. U.; Pak, Y. E.; Colla, E. L.; Setter, N.; Kim, E.; No, K. Principle of Ferroelectric Domain Imaging Using Atomic Force Microscope. *J. Appl. Phys.* **2001**, *89*, 1377–1386.
48. Sugiyama, I.; Kim, Y.; Jesse, S.; Strelcov, E.; Kumar, A.; Tselev, A.; Rahani, E. K.; Shenoy, V. B.; Yamamoto, T.; Shibata, N.; et al. Spatially-Resolved Mapping of History-Dependent Coupled Electrochemical and Electronical Behaviors of Electroresistive NiO. *Sci. Rep.* **2014**, *4*, 6725.
49. Kumar, A.; Arruda, T. M.; Kim, Y.; Ivanov, I. N.; Jesse, S.; Bark, C. W.; Bristowe, N. C.; Artacho, E.; Littlewood, P. B.; Eom, C.-B.; et al. Probing Surface and Bulk Electrochemical

Processes on the $LaAlO_3$−$SrTiO_3$ Interface. *ACS Nano* **2012**, *6*, 3841–3852.
50. Kim, Y.; Strelcov, E.; Hwang, I. R.; Choi, T.; Park, B. H.; Jesse, S.; Kalinin, S. V. Correlative Multimodal Probing of Ionically-Mediated Electromechanical Phenomena in Simple Oxides. *Sci. Rep.* **2013**, *3*, 2924.
51. Kim, Y.; Jang, J. H.; Park, S.-J.; Jesse, S.; Donovan, L.; Borisevich, A. Y.; Lee, W.; Kalinin, S. V. Local Probing of Electrochemically Induced Negative Differential Resistance in TiO_2 Memristive Materials. *Nanotechnology* **2013**, *24*, 085702.
52. Kumar, A.; Ciucci, F.; Morozovska, A. N.; Kalinin, S. V.; Jesse, S. Measuring Oxygen Reduction/Evolution Reactions on the Nanoscale. *Nat. Chem.* **2011**, *3*, 707–713.
53. Clima, S.; Wouters, D. J.; Adelmann, C.; Schenk, T.; Schroeder, U.; Jurczak, M.; Pourtois, G. Identification of the Ferroelectric Switching Process and Dopant-Dependent Switching Properties in Orthorhombic HfO_2: A First Principles Insight. *Appl. Phys. Lett.* **2014**, *104*, 092906.
54. Zhou, D. Y.; Xu, J.; Li, Q.; Guan, Y.; Cao, F.; Dong, X. L.; Muller, J.; Schenk, T.; Schroder, U. Wake-up Effects in Si-Doped Hafnium Oxide Ferroelectric Thin Films. *Appl. Phys. Lett.* **2013**, *103*, 192904.
55. Mueller, S.; Mueller, J.; Singh, A.; Riedel, S.; Sundqvist, J.; Schroeder, U.; Mikolajick, T. Incipient Ferroelectricity in Al-Doped HfO_2 Thin Films. *Adv. Funct. Mater.* **2012**, *22*, 2412–2417.
56. Muller, J.; Schroder, U.; Boscke, T. S.; Muller, I.; Bottger, U.; Wilde, L.; Sundqvist, J.; Lemberger, M.; Kucher, P.; Mikolajick, T.; et al. Ferroelectricity in Yttrium-Doped Hafnium Oxide. *J. Appl. Phys.* **2011**, *110*, 114113.
57. Muller, J.; Boscke, T. S.; Schroder, U.; Mueller, S.; Brauhaus, D.; Bottger, U.; Frey, L.; Mikolajick, T. Ferroelectricity in Simple Binary ZrO_2 and HfO_2. *Nano Lett.* **2012**, *12*, 4318–4323.
58. Jang, H. W.; Kumar, A.; Denev, S.; Biegalski, M. D.; Maksymovych, P.; Bark, C. W.; Nelson, C. T.; Folkman, C. M.; Baek, S. H.; Balke, N.; et al. Ferroelectricity in Strain-Free $SrTiO_3$ Thin Films. *Phys. Rev. Lett.* **2010**, *104*, 197601.
59. Strelcov, E.; Kim, Y.; Yang, J. C.; Chu, Y. H.; Yu, P.; Lu, X.; Jesse, S.; Kalinin, S. V. Role of Measurement Voltage on Hysteresis Loop Shape in Piezoresponse Force Microscopy. *Appl. Phys. Lett.* **2012**, *101*, 192902.
60. Morozovska, A. N.; Eliseev, E. A.; Svechnikov, G. S.; Kalinin, S. V. Nanoscale Electromechanics of Paraelectric Materials with Mobile Charges: Size Effects and Nonlinearity of Electromechanical Response of $SrTiO_3$ Films. *Phys. Rev. B* **2011**, *84*, 045402.
61. Jesse, S.; Kalinin, S. V.; Proksch, R.; Baddorf, A. P.; Rodriguez, B. J. The Band Excitation Method in Scanning Probe Microscopy for Rapid Mapping of Energy Dissipation on the Nanoscale. *Nanotechnology* **2007**, *18*, 435503.